Letter

# Disorder-induced instability of a Weyl nodal loop semimetal towards a diffusive topological metal with protected multifractal surface states

João S. Silva [1], Miguel Gonçalves [2], Eduardo V. Castro [1,3], Pedro Ribeiro [2,3] and Miguel A. N. Araújo [3,4,5]

[1] *Centro de Física das Universidades do Minho e Porto, LaPMET, Departamento de Física e Astronomia, Faculdade de Ciências, Universidade do Porto, P-4169-007 Porto, Portugal*

[2] *CeFEMA, LaPMET, Instituto Superior Técnico, Universidade de Lisboa, Avenida Rovisco Pais, P-1049-001 Lisboa, Portugal*

[3] *Beijing Computational Science Research Center, Beijing 100193, China*

[4] *CeFEMA, Instituto Superior Técnico, Universidade de Lisboa, Avenida Rovisco Pais, P-1049-001 Lisboa, Portugal*

[5] *Departamento de Física, Universidade de Évora, P-7000-671 Évora, Portugal*

(Received 29 April 2024; revised 19 November 2024; accepted 21 January 2025; published 28 January 2025)

Weyl nodal loop semimetals are gapless topological phases that, unlike their insulator counterparts, may be unstable to small perturbations that respect their topology-protecting symmetries. Here, we analyze a clean system perturbed by chiral off-diagonal disorder using numerically exact methods. We establish that the ballistic semimetallic phase is unstable towards the formation of an unconventional topological diffusive metal hosting topological multifractal surface states. Although, as in the clean case, surface states are exponentially localized along the direction perpendicular to the nodal loop, disorder induces a multifractal structure in the remaining directions. Surprisingly, the number of these states also increases with a small amount of disorder. Eventually, as disorder is further increased, the number of surface states starts decreasing.

DOI: 10.1103/PhysRevB.111.L041116

The topological properties of quantum matter are robust to small perturbations, such as weak disorder. As long as the clean limit symmetries are preserved, bulk topological characteristics and associated boundary states survive until a critical disorder threshold is reached, where a topological transition takes place. Particularly interesting examples of these phases are first-order [1,2] and higher-order [3,4] topological insulators, which, in certain cases, only require disorder to preserve the clean limit symmetries on average [5], rendering them particularly robust and appealing for applications.

Recently, topological semimetals stood out as an important class of three-dimensional (3D) topological materials not requiring a gap [6–9]. Weyl nodal loop (WNL) semimetals, in particular, are characterized by a linearly vanishing density of states (DOS) due to the linear touch of conduction and valence bands along a loop or line in momentum space [10]. Their nontrivial bulk topology gives rise to characteristic surface states—the so-called drumhead states—which have been detected recently by a variety of methods in different materials [11–16]. This calls for a deeper understanding on the effect of disorder on the topological phase diagram of these systems.

Interesting consequences of symmetry-breaking disorder were reported in Refs. [17,18]. However, the case of disorder that preserves the underlying symmetry, such as a WNL semimetal subjected to chiral symmetric disorder, is particularly intriguing, and remains open. On one hand, chiral disorder is known to induce an enhanced DOS at zero energy in chiral symmetric models [19,20], which in two dimensions even becomes logarithmically divergent [21], casting doubts on the stability of the semimetallic phase. On the other hand, since the symmetry remains unbroken, the robustness of bulk topological properties and accompanying drumhead states are still expected, suggesting the stability of the topological semimetal to weak disorder. In this Letter, we solve this apparent contradiction.

By considering a generic model for a chiral symmetric WNL, we show that the semimetallic phase is unstable to chiral disorder, and a finite DOS at zero energy is always present. However, the induced metallic phase is accompanied by a quantized, nontrivial winding number, and by zero-energy edge states which, for weak disorder, are higher in number than the clean limit drumhead surface states. The winding number $\nu$, which in the clean limit counts the number of $\boldsymbol{k}$ points inside the nodal loop, is shown in Fig. 1(a) versus the disorder strength $W$. Adding chiral disorder makes this topological invariant increase, which is accompanied by an increase of the estimated number of surface states $\tilde{\nu}$, depicted in Fig. 1(b). At the same time, the presence of a finite zero-energy DOS for any finite disorder, as shown in the inset of Fig. 1(a), clearly points to a diffusive metallic phase [22]. By further increasing the disorder strength, both $\nu$ and $\tilde{\nu}$ fade away for general chiral disorder, but a topological transition does not occur.

The presence of nontrivial topology and boundary states together with a finite bulk DOS at the Fermi energy shows that the WNL is unstable to a topological metal phase under chiral disorder. However, unlike previously known topological metals [23–28], chiral disorder is an essential ingredient since the system is a semimetal in the clean limit. Moreover, the surface states of this topological metal acquire a multifractal structure in real space, in contrast to the clean WNL and to models with disorder in one spatial direction [17]. This is an instance of a system hosting topological multifractal surface states, which realize a different type of bound states in the continuum [29–33].

 

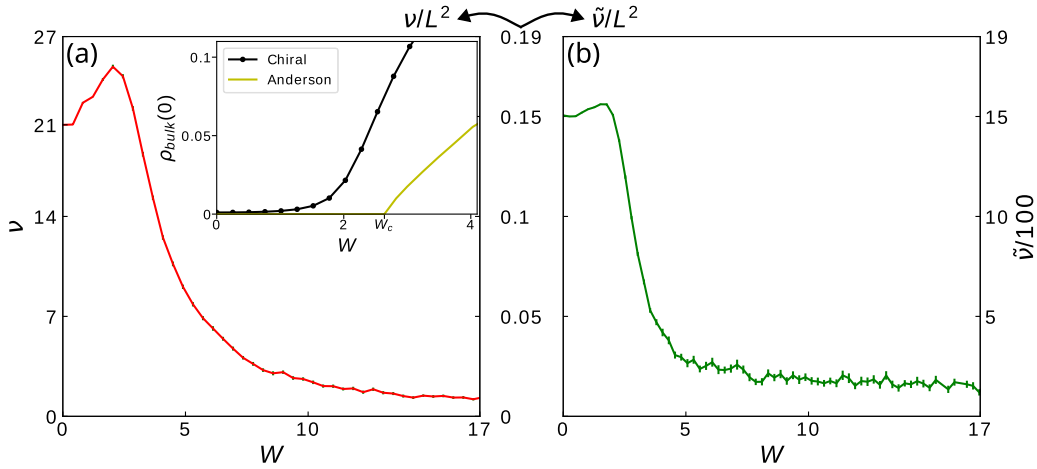


FIG. 1. (a) Winding number vs chiral disorder strength for a system with $L^3 = 12^3$ unit cells. The inset shows that a finite DOS at zero energy appears with increasing disorder, signaling a metallic phase in contrast with Anderson disorder [18]. (b) Estimated number of surface states ($\tilde{\nu}$) vs disorder obtained with KPM for $L = 100$ and $N_m = 2^{10}$ [$L = 200$ and $N_m = 2^{11}$ for the DOS in the inset of (a)].

We consider a two-band model on a cubic lattice with $L^3$ cells and disorder [18,34],

$$\hat{H} = \sum_{\boldsymbol{k}} c_{\boldsymbol{k}}^{\dagger} H_{\boldsymbol{k}} c_{\boldsymbol{k}} + \hat{V}. \tag{1}$$

The first term describes a clean WNL [18], with $\boldsymbol{k}$ a 3D Bloch vector, $H_{\boldsymbol{k}} = (t_x \cos k_x + t_y \cos k_y + \cos k_z - m)\tau_x + t_2 \sin k_z \tau_y$, with $\tau_x, \tau_y$ Pauli matrices acting on the orbital pseudospin indices $\alpha = 1, 2$, and $c_{\boldsymbol{k}}^{\dagger} = (c_{\boldsymbol{k},1}^{\dagger} \quad c_{\boldsymbol{k},2}^{\dagger})$. In the following, we make the parameter choice $t_x = 1.1$, $t_y = 0.9$, $m = 2.12$, and $t_2 = 0.8$. This choice yields a single nodal line, arising for $k_z = 0$, with the equation $t_x \cos k_x + t_y \cos k_y + 1 - m = 0$. The number of $\boldsymbol{k}$ points inside the nodal loop is the number of drumhead states in a clean WNL [11,17,18,34–40]. The second term is the off-diagonal disorder. In real space, it reads

$$\hat{V} = \sum_{\boldsymbol{r}} \left[ \left( \frac{1}{2} \sum_{\delta = x,y,z} V_{\boldsymbol{r}}^{\delta} c_{\boldsymbol{r}}^{\dagger} \tau_x c_{\boldsymbol{r}+\boldsymbol{e}_\delta} + \text{H.c.} \right) + V_{\boldsymbol{r}}^{0} c_{\boldsymbol{r}}^{\dagger} \tau_x c_{\boldsymbol{r}} \right], \tag{2}$$

where $V_{\boldsymbol{r}}^{\delta} = W \omega_{\boldsymbol{r}}^{\delta}$, with four independent random numbers $\omega_{\boldsymbol{r}}^{\delta} \in [-\frac{1}{2}, \frac{1}{2}]$, with $\delta = 0, x, y, z$. $W$ measures the disorder strength. The model in Eq. (1) realizes a chiral symmetric disordered WNL. We later also consider the case of intracell chiral disorder, where $\omega_{\boldsymbol{r}}^{\delta} = 0$ for $\delta \neq 0$. Unless otherwise stated, our results are averaged over 100 disorder realizations.

For a disordered chiral system, a winding number $\nu$ can be calculated from real-space wave functions through the coupling matrix approach [41,42], by applying twisted boundary conditions along the $z$ direction. For a given twist angle $\theta$ the ground-state many-body wave function for a half-filled system, $|\Phi(\theta)\rangle$, is a Slater determinant of single-particle states, $|\psi_j(\theta)\rangle$, and the overlap $\langle \Phi(\theta)|\Phi(\theta')\rangle = \text{Det}[\langle \psi_j(\theta)|\psi_{j'}(\theta')\rangle]$. Then, $\nu$ obeys $e^{i\pi\nu} = \Pi_{\theta=0}^{\theta=2\pi-d\theta} \langle \Phi(\theta)|\Phi(\theta + d\theta)\rangle$ where $\Phi(2\pi) = \Phi(0)$. In practice, the matrix product $\Pi_{\theta=0}^{\theta=2\pi-d\theta} \langle \Phi(\theta)|\Phi(\theta + d\theta)\rangle$ is computed and the sum of the phases of its eigenvalues yields the value of $\pi\nu$. According to the bulk boundary correspondence principle, the winding number yields the number of surface states (SSs). In a clean WNL, $\nu$ equals the number of drumhead states, as seen in Fig. 1(a) for $W = 0$ (where $L = 12$ implies exactly 21 drumhead states).

The winding number as a function of increasing disorder is shown in Fig. 1(a), where it can be seen to increase with disorder for $W \lesssim 2$. A transition to a topologically trivial phase where $\nu = 0$ is not observed. Instead, we find that the disorder averaged winding number exhibits a power-law decay $\nu \propto W^{\alpha}$, with $\alpha \approx -1.9$ fairly insensitive to the system's size, as illustrated in Fig. 2(a). The finite winding number at finite chiral disorder is concomitant with a finite bulk DOS at zero energy, as shown in the inset of Fig. 1(a) alongside the DOS for the Anderson diagonal disorder, where a semimetal-to-metal transition takes place at $W_c$ [18]. For any finite chiral disorder, the system is both topologically nontrivial and a metal.

Counting the number of surface states as chiral disorder increases would require treating exactly a semi-infinite system, thus avoiding surface-state hybridization on opposite boundaries. For the numerically exact approach we have been following, surfaces are created in pairs, so the presence of at least two is unavoidable. To minimize the mentioned hybridization, we use a method which allows to reach large system sizes: We study the change in the DOS that occurs when periodic boundary conditions (PBCs) along the $z$ direction are replaced by open boundary conditions (OBCs) [34]. Then, any change in the DOS must be a surface effect. We define the density of surface states, $\Delta\rho(E) \equiv \rho_{\text{OBC}}(E) - \rho_{\text{PBC}}(E)$, where $\rho_{\text{PBC}}$ ($\rho_{\text{OBC}}$) denotes the DOS calculated for PBCs (OBCs) along the $z$ direction. The integral of $\Delta\rho(E)$ over the whole energy axis vanishes because the total number of states ($2L^3$) is the same for OBCs and PBCs: Bulk states are destroyed to compensate for the creation of edge states. The number of low-energy surface states for OBCs can be estimated by defining the energy interval, $|E| < E_w$, around zero energy where $\Delta\rho(E) > 0$. Then, the integral

$$\tilde{\nu} = L^3 \int_{-E_w}^{E_w} \Delta\rho(E) dE \tag{3}$$

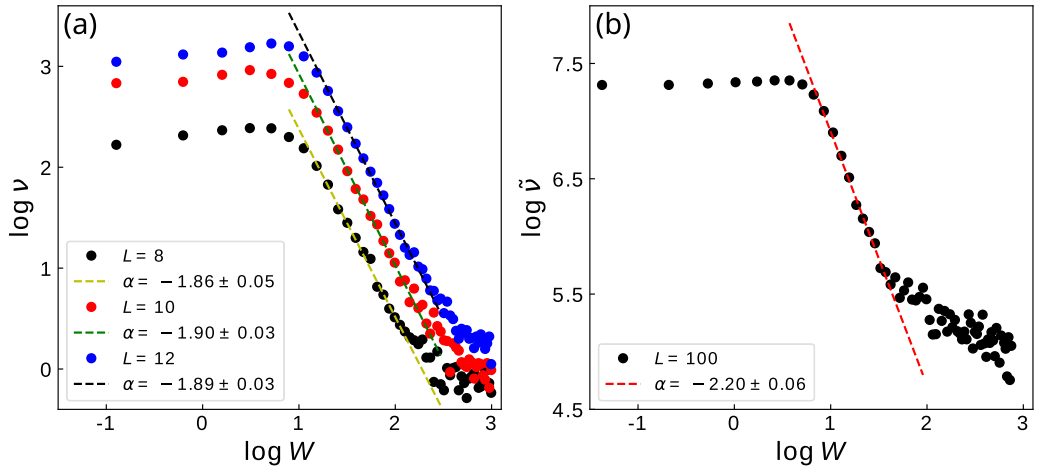


FIG. 2. Log-log plots for the data shown in Fig. 1: (a) Disorder averaged winding number per unit area, $\nu/L^2$, vs disorder strength $W$ for clusters of $L^3$ cells; (b) estimated number of low-energy surface states $\tilde{\nu}$ vs $W$, obtained using $N_m = 2^{10}$ polynomials for a system with $100^3$ cells. Dashed lines are linear fits to the data.

provides an estimation of the number of low-energy surface states. We compute the DOS using the kernel polynomial method (KPM) with an expansion in Chebyshev polynomials to order $N_m$ [43].

The results for $\tilde{\nu}$ are presented in Fig. 1(b) and reveal an enhancement for $W \lesssim 2$, in agreement with the winding number in Fig. 1(a). For higher disorder, $\tilde{\nu}$ decays as a power law, as the winding number $\nu$, but with a different exponent $\alpha = -2.20 \pm 0.06$, which indicates that $\tilde{\nu} < \nu$. In fact, we should expect $\tilde{\nu}$ to be a lower bound for the true number of drumhead states, even in the absence of disorder: This is because the edge states near the nodal line (where their localization length diverges) hybridize with others on the opposite surface. The resulting energy splitting shifts their energies to values higher than $E_w$, outside the integration domain in Eq. (3).

The low disorder enhancement of surface states can be understood if we consider the conceptually simpler case of disorder in one spatial direction, where the random hopping terms only spatially depend on the $z$ coordinate, by setting $\omega_{\boldsymbol{r}}^x = \omega_{\boldsymbol{r}}^y = \omega_{\boldsymbol{r}}^0 = 0$ in Eq. (2). The system then behaves as a set of decoupled chains along the $z$ axis, each labeled by $(k_x, k_y)$. Each chain has a winding number, $\nu(k_x, k_y)$, which is unity inside the nodal loop, and zero outside, in the clean case. Each chain then undergoes a chiral disorder-induced topological transition in 1D [44]. Figures 3(a)–3(d) show the disorder averaged $\nu(k_x, k_y)$ at different disorder values. It is seen that weak disorder slightly enlarges the area of the central region. In this case, the total winding number $\nu$ is given by $\nu = \sum_{k_x,k_y} \nu(k_x, k_y)$, and it is clearly enhanced for $W \lesssim 2$, as shown in Fig. 3(e). The physical interpretation is that the $(k_x, k_y)$ trivial chains just outside the nodal line, which are close to a 1D topological transition, become topological under weak disorder, as observed in topological Anderson insulators [45,46]. At stronger disorder, $W \gtrsim 2$, the chains gradually transit to the trivial phase, starting from the periphery towards the inside. Figure 3(e) also shows that $\nu$ vanishes above a critical disorder strength, as expected, signaling that all the chains (the 3D system) are topologically trivial.

For the full 3D disordered case shown in Fig. 1(a), no quantum states can be labeled by momentum. However, the enhancement of $\nu$ at $W \lesssim 2$ shows that some bulk quantum states are close to becoming surface states upon adding weak disorder, a feature shared with the case of disorder in one spatial direction. The difference to disorder in one spatial direction, here, is that no topological to trivial transition is observed at high $W$. The degree of enhancement of $\nu/L^2$ can be increased or decreased by changing the model parameters.

The presence of chiral symmetry and the existence of a winding number imply that the associated surface states decay exponentially into the bulk. In the clean limit, exponential localization of drumhead states is well understood using, for example, the decomposition in decoupled chains along $z$ mentioned above. In the following we demonstrate that, for the chiral disordered system, localization of surface states also takes place. The decay of probability into the bulk can be found from an inverse participation ratio (IPR) defined for the $z$ direction in sublattice $\alpha$ as

$$\mathrm{IPR}_z^\alpha = \frac{\sum_z \Psi^4(z,\alpha)}{\left[\sum_z \Psi^2(z,\alpha)\right]^2}, \tag{4}$$

where the probability $\Psi^2(z,\alpha) = \sum_{x,y} |\psi(x,y,z;\alpha)|^2$ is obtained from the surface-state wave function $\psi(\boldsymbol{r},\alpha)$. Figure 4(a) shows the exponential decay of the lowest-energy surface-state probability from the $z = 1$ surface. Disorder *increases* the localization length $\xi$ in the range of $W$ considered. This is confirmed in Fig. 4(b), where $\mathrm{IPR}_z^\alpha$ is a decreasing function of $W$. This behavior is akin to the problem in 1D [44]. It also explains why $\tilde{\nu}$ decreases faster than $\nu$: Since $\xi$ increases with $W$, a larger fraction of surface states on opposite sides of the sample significantly hybridize at larger $W$, falling out of the integration energy window $E_w$ in Eq. (3). The inset to Fig. 4(b) shows that the $\mathrm{IPR}_z^\alpha$ monotonous dependence on $L$ inverts at $W \gtrsim 8.5$. At this disorder value, the localization length exceeds the system sizes considered, pointing to a finite-size effect. The inset also shows that the crossing point between consecutive sizes, signaled by the open circles,

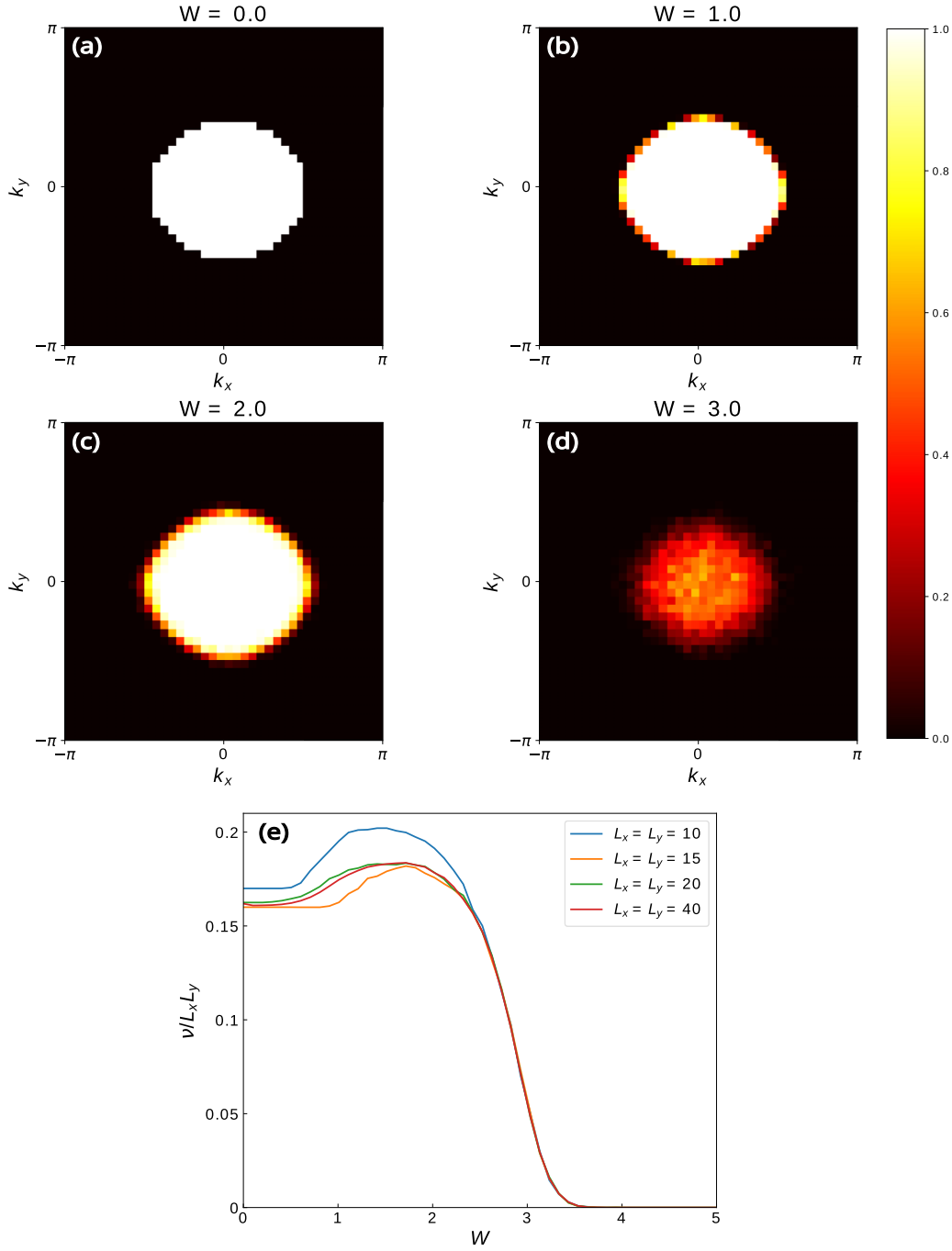


FIG. 3. (a)–(d) Momentum-resolved winding number, $\nu(k_x, k_y)$, for increasing disorder values $W$. (e) Disorder averaged total winding number per unit area vs disorder strength. The system's length along $z$ is 100 unit cells.

shifts to higher disorder as $L$ increases, in agreement with this scenario.

To gain a deeper understanding on the localization of surface states we investigate their multifractal structure. This is done in real space through the generalized IPR for a system with linear size $L$,

$$\mathcal{I}(q) = \frac{\sum_{\mathbf{r},\alpha} |\psi(\mathbf{r},\alpha)|^{2q}}{\left(\sum_{\mathbf{r},\alpha} |\psi(\mathbf{r},\alpha)|^{2}\right)^{q}} \propto L^{-\tau(q)}, \tag{5}$$

where $\psi(\mathbf{r},\alpha)$ is the lowest-energy surface state amplitude at cell $\mathbf{r}$ and sublattice $\alpha$. Writing the exponent as $\tau(q) = D(q)\cdot(q-1)$, a constant $D(q) = D$ defines the fractal dimension of the wave function. If $D(q)$ is not constant, the wave function is said to be multifractal [47]. In Fig. 4(c) it can be seen that $\tau(q)$ is nonlinear for $W \neq 0$, implying the multifractality of surface states. Focusing on the $q = 2$ case, the quantity $\mathcal{I}(2)$ in Eq. (5) becomes the IPR. The scaling exponent IPR $\propto L^{\beta}$, with $\beta = -\tau(2)$, is shown in Fig. 4(d) as a function of the disorder strength $W$. For the $W = 0$ (clean limit), we obtain the exponent $\beta = -2$ as expected for a surface state that extends in the $xy$ surface and is localized along $z$. However, for $W \neq 0$, the exponent reveals a highly nontrivial fractal dimension dependence on disorder.

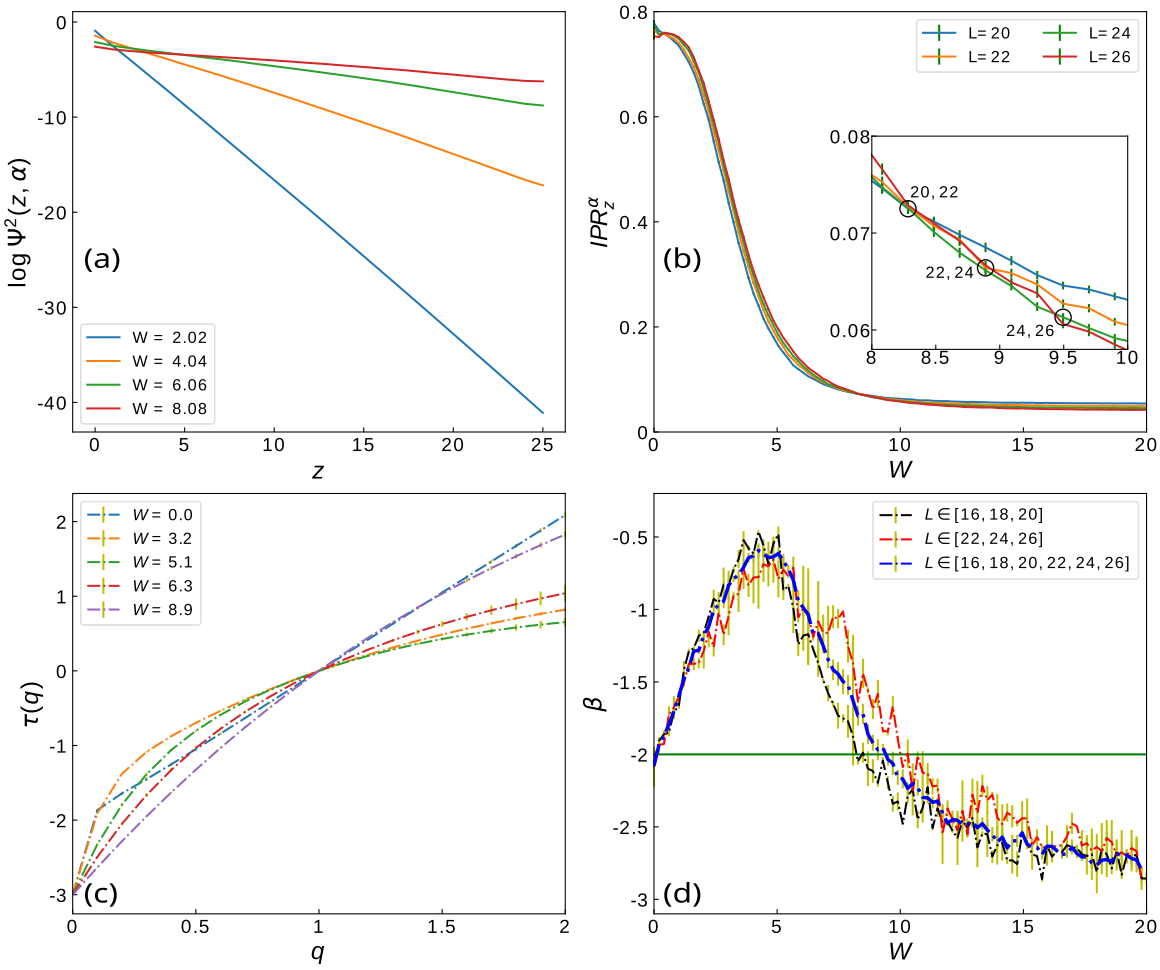


FIG. 4. Localization properties of the lowest-energy surface state: (a) Exponential decay of probability $|\Psi(z,\alpha)|^2$ into the bulk for sublattice $\alpha = 1$; (b) $\mathrm{IPR}_z^\alpha$ vs disorder strength $W$ for various system sizes $L$; (c) $\tau(q)$ for various $W$; (d) IPR scaling exponent $\beta = -\tau(2)$ vs $W$.

For high disorder, $W \gtrsim 10$, the slope of $\tau(q)$ becomes approximately 3 [$D(q) \approx 3$], indicating that the probability occupies the full three-dimensional volume. This is already apparent for $W = 8.9$ in Fig. 4(c), particularly at low $q$. We believe that this is because the localization length exceeds $L$ and that this behavior breaks down for large enough systems. The value $|\beta| > 2$ for $W \gtrsim 8.5$ in Fig. 4(d) is also likely due to $\xi$ exceeding the system sizes considered. Notice that in Fig. 4(d) the $W$ value at which $|\beta| \approx 2$ increases if we consider only the largest sizes. Other low-energy states present the same features shown in Fig. 4.

We now turn to the case where only the intracell hopping term $m$ is disordered ($\omega_r^\delta = 0$, except if $\delta = 0$). Two qualitative differences to the previous fully disordered case are found: an exponential decrease of $\nu$ with disorder strength, as seen in Figs. 5(a) and 5(b), with similar results for $\tilde{\nu}$ (not shown); and Fig. 5(c) suggests an Anderson localization transition at higher $W$ [22], which we have confirmed with the transfer matrix method (not shown) [48], and does not exist in the previous case. We find that for a disorder strength $15 \lesssim W \lesssim 18$ the system is in a quasilocalized phase [48,49]. However, unlike Ref. [48], we do not see the winding number vanish after the Anderson transition, which, we believe, is due to finite-size effects. Since, in Fig. 4(b), we do not find an Anderson transition, we believe that a quasilocalized phase is not present in the fully disordered model.

The dependence of the localization length of surface states on disorder is also more complex. Figure 5(c) for $\mathrm{IPR}_z^\alpha$ shows that $\xi$ first decreases ($W \lesssim 2$), then increases ($2 \lesssim W \lesssim 12$), and finally decreases beyond $W \gtrsim 12$, indicative of proximity to an Anderson transition. The exponent $\tau(q)$, shown in Fig. 5(d), exhibits multifractal behavior.

In summary, we have established the fate of a WNL semimetal under the presence of chiral disorder and shown that the semimetallic phase is unstable to a topological metal. The coexistence of topological surface and bulk extended states of the disordered metal is a consequence of the finite winding number, in agreement with the bulk-edge correspondence principle. The surface states are robust up to very large disorder, decaying exponentially into the bulk in the direction orthogonal to the nodal loop. They exhibit multifractal properties along the surface that strongly and nontrivially depend on disorder strength, thus realizing a different type of bound

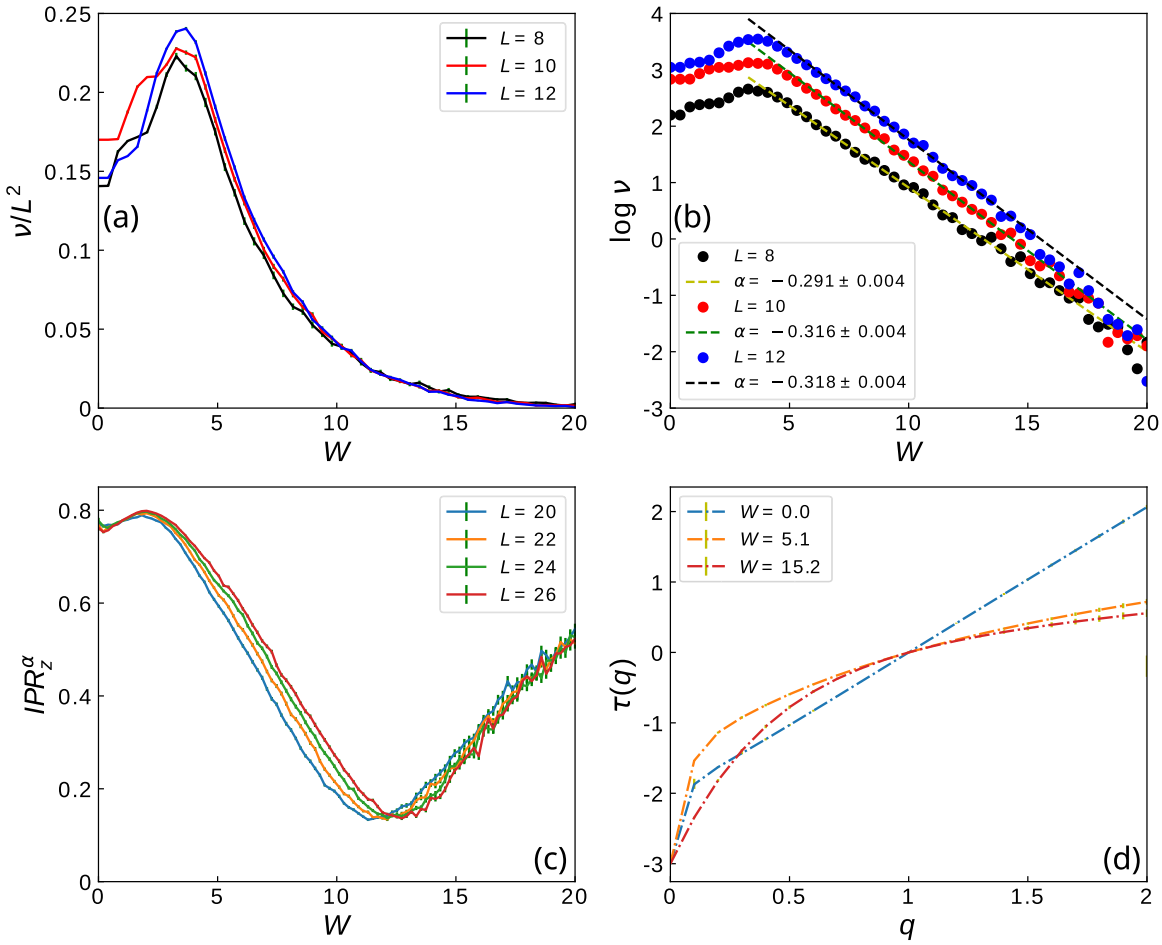


FIG. 5. (a) Disorder averaged winding number per unit area, $\nu/L^2$, vs intracell disorder $W$ for clusters of $L^3$ sites. (b) Log-linear plot for the data in (a). (c) $\mathrm{IPR}_z^\alpha$ vs disorder strength $W$ for various system sizes $L$. (d) $\tau(q)$ for various $W$.

states in the continuum [29–33]. This is an example of a 3D intrinsically disordered topological metal. The observable signatures of this exotic state of matter, such as transport properties, should be investigated in the future.

M.G., P.R., and M.A. acknowledge partial support from Fundação para a Ciência e Tecnologia (FCT-Portugal) through Grant No. UID/CTM/04540/2019. M.G. and E.V.C. acknowledge partial support from FCT-Portugal through Grant No. UIDB/04650/2020. M.G. acknowledges further support from FCT-Portugal through Grant No. SFRH/BD/145152/2019. We finally acknowledge the Tianhe-2JK cluster at the Beijing Computational Science Research Center (CSRC) and the OBLIVION supercomputer (based at the High Performance Computing Center - University of Évora) funded by the ENGAGE SKA Research Infrastructure (Ref. No. POCI-01-0145-FEDER-022217 - COMPETE 2020 and the Foundation for Science and Technology, Portugal) and by the BigData@UE project (Ref. No. ALT20-03-0246-FEDER-000033 - FEDER) and the Alentejo 2020 Regional Operational Program. Computer assistance was provided by CSRC, CENTRA/IST and the OBLIVION support team.

[1] C. K. Chiu, J. C. Y. Teo, A. P. Schnyder, and S. Ryu, Classification of topological quantum matter with symmetries, Rev. Mod. Phys. **88**, 035005 (2016).

[2] T. Okugawa, T. Nag, and D. M. Kennes, Correlated disorder induced anomalous transport in magnetically doped topological insulators, Phys. Rev. B **106**, 045417 (2022).

[3] C. A. Li, B. Fu, Z. A. Hu, J. Li, and S. Q. Shen, Topological phase transitions in disordered electric quadrupole insulators, Phys. Rev. Lett. **125**, 166801 (2020).

[4] W. A. Benalcazar and A. Cerjan, Chiral-symmetric higher-order topological phases of matter, Phys. Rev. Lett. **128**, 127601 (2022).

[5] Z.-D. Song, B. Lian, R. Queiroz, R. Ilan, B. A. Bernevig, and A. Stern, Delocalization transition of a disordered axion insulator, Phys. Rev. Lett. **127**, 016602 (2021).

[6] N. P. Armitage, E. J. Mele, and A. Vishwanath, Weyl and Dirac semimetals in three-dimensional solids, Rev. Mod. Phys. **90**, 015001 (2018).

[7] S. Klemenz, S. Lei, and L. M. Schoop, Topological semimetals in square-net materials, Annu. Rev. Mater. Res. **49**, 185 (2019).

[8] R.-J. Slager, V. Juričić, and B. Roy, Dissolution of topological Fermi arcs in a dirty Weyl semimetal, Phys. Rev. B **96**, 201401(R) (2017).

[9] B. Roy, R.-J. Slager, and V. Juričić, Global phase diagram of a dirty Weyl liquid and emergent superuniversality, Phys. Rev. X **8**, 031076 (2018).

[10] R. Yu, Z. Fang, X. Dai, and H. Weng, Topological nodal line semimetals predicted from first-principles calculations, Front. Phys. **12**, 127202 (2017).

[11] G. Bian, T.-R. Chang, R. Sankar, S.-Y. Xu, H. Zheng, T. Neupert, C.-K. Chiu, S.-M. Huang, G. Chang, I. Belopolski, D. S. Sanchez, M. Neupane, N. Alidoust, C. Liu, B. Wang, C.-C. Lee, H.-T. Jeng, C. Zhang, Z. Yuan, S. Jia *et al.*, Topological nodal-line fermions in spin-orbit metal $PbTaSe_2$, Nat. Commun. **7**, 10556 (2016).

[12] I. Belopolski, K. Manna, D. S. Sanchez, G. Chang, B. Ernst, J. Yin, S. S. Zhang, T. Cochran, N. Shumiya, H. Zheng, B. Singh, G. Bian, D. Multer, M. Litskevich, X. Zhou, S.-M. Huang, B. Wang, T.-R. Chang, S.-Y. Xu, A. Bansil *et al.*, Discovery of topological Weyl fermion lines and drumhead surface states in a room temperature magnet, Science **365**, 1278 (2019).

[13] L. Muechler, A. Topp, R. Queiroz, M. Krivenkov, A. Varykhalov, J. Cano, C. R. Ast, and L. M. Schoop, Modular arithmetic with nodal lines: Drumhead surface states in ZrSiTe, Phys. Rev. X **10**, 011026 (2020).

[14] C. Sims, M. M. Hosen, H. Aramberri, C.-Y. Huang, G. Dhakal, K. Dimitri, F. Kabir, S. Regmi, X. Zhou, T.-R. Chang, H. Lin, D. Kaczorowski, N. Kioussis, and M. Neupane, Termination-dependent topological surface states in nodal-loop semimetal $HfP_2$, Phys. Rev. Mater. **4**, 054201 (2020).

[15] M. M. Hosen, G. Dhakal, B. Wang, N. Poudel, K. Dimitri, F. Kabir, C. Sims, S. Regmi, K. Gofryk, D. Kaczorowski, A. Bansil, and M. Neupane, Experimental observation of drumhead surface states in $SrAs_3$, Sci. Rep. **10**, 2776 (2020).

[16] B. A. Stuart, S. Choi, J. Kim, L. Muechler, R. Queiroz, M. Oudah, L. M. Schoop, D. A. Bonn, and S. A. Burke, Quasiparticle interference observation of the topologically nontrivial drumhead surface state in ZrSiTe, Phys. Rev. B **105**, L121111 (2022).

[17] Y. Wang, H. Hu, and S. Chen, Effect of an incommensurate potential on nodal-link semimetals, Phys. Rev. B **98**, 205410 (2018).

[18] M. Gonçalves, P. Ribeiro, E. V. Castro, and M. A. N. Araújo, Disorder-driven multifractality transition in Weyl nodal loops, Phys. Rev. Lett. **124**, 136405 (2020).

[19] S. N. Evangelou and D. E. Katsanos, Spectral statistics in chiral-orthogonal disordered systems, J. Phys. A: Math. Gen. **36**, 3237 (2003).

[20] A. M. García-García and E. Cuevas, Anderson transition in systems with chiral symmetry, Phys. Rev. B **74**, 113101 (2006).

[21] R. Gade, Anderson localization for sublattice models, Nucl. Phys. B **398**, 499 (1993).

[22] X. Luo, B. Xu, T. Ohtsuki, and R. Shindou, Critical behavior of Anderson transitions in three-dimensional orthogonal classes with particle-hole symmetries, Phys. Rev. B **101**, 020202(R) (2020).

[23] X. Ying and A. Kamenev, Symmetry-protected topological metals, Phys. Rev. Lett. **121**, 086810 (2018).

[24] M. Bahari and M. V. Hosseini, One-dimensional topological metal, Phys. Rev. B **99**, 155128 (2019).

[25] M. Jangjan and M. V. Hosseini, Topological phase transition between a normal insulator and a topological metal state in a quasi-one-dimensional system, Sci. Rep. **11**, 12966 (2021).

[26] L. C. Xie, H. C. Wu, L. Jin, and Z. Song, Time-reversal symmetric topological metal, Phys. Rev. B **104**, 165422 (2021).

[27] A. Cerjan and T. A. Loring, Local invariants identify topology in metals and gapless systems, Phys. Rev. B **106**, 064109 (2022).

[28] L. Xie, L. Jin, and Z. Song, Antihelical edge states in two-dimensional photonic topological metals, Sci. Bull. **68**, 255 (2023).

[29] B.-J. Yang, M. Saeed Bahramy, and N. Nagaosa, Topological protection of bound states against the hybridization, Nat. Commun. **4**, 1524 (2013).

[30] C. W. Hsu, B. Zhen, A. D. Stone, J. D. Joannopoulos, and M. Soljačić, Bound states in the continuum, Nat. Rev. Mater. **1**, 16048 (2016).

[31] Y.-X. Xiao, G. Ma, Z.-Q. Zhang, and C. T. Chan, Topological subspace-induced bound state in the continuum, Phys. Rev. Lett. **118**, 166803 (2017).

[32] Z.-G. Chen, C. Xu, R. Al Jahdali, J. Mei, and Y. Wu, Corner states in a second-order acoustic topological insulator as bound states in the continuum, Phys. Rev. B **100**, 075120 (2019).

[33] W. A. Benalcazar and A. Cerjan, Bound states in the continuum of higher-order topological insulators, Phys. Rev. B **101**, 161116(R) (2020).

[34] J. S. Silva, M. A. N. Araújo, M. Gonçalves, P. Ribeiro, and E. V. Castro, Delocalization of topological surface states by diagonal disorder in nodal loop semimetals, Phys. Rev. B **107**, 045146 (2023).

[35] R. Yu, H. Weng, Z. Fang, X. Dai, and X. Hu, Topological node-line semimetal and Dirac semimetal state in antiperovskite $Cu_3PdN$, Phys. Rev. Lett. **115**, 036807 (2015).

[36] Y. Kim, B. J. Wieder, C. L. Kane, and A. M. Rappe, Dirac line nodes in inversion-symmetric crystals, Phys. Rev. Lett. **115**, 036806 (2015).

[37] H. Weng, Y. Liang, Q. Xu, R. Yu, Z. Fang, X. Dai, and Y. Kawazoe, Topological node-line semimetal in three-dimensional graphene networks, Phys. Rev. B **92**, 045108 (2015).

[38] L. Li, C. Yin, S. Chen, and M. A. N. Araújo, Chiral topological insulating phases from three-dimensional nodal loop semimetals, Phys. Rev. B **95**, 121107(R) (2017).

[39] L. Li, H. H. Yap, M. A. N. Araújo, and J. Gong, Engineering topological phases with a three-dimensional nodal-loop semimetal, Phys. Rev. B **96**, 235424 (2017).

[40] M. A. N. Araújo and P. D. Sacramento, *Topology in Condensed Matter: An Introduction* (World Scientific, Singapore, 2021).

[41] Y.-F. Zhang, Y.-Y. Yang, Y. Ju, L. Sheng, R. Shen, D.-N. Sheng, and D.-Y. Xing, Coupling-matrix approach to the Chern number calculation in disordered systems, Chin. Phys. B **22**, 117312 (2013).

[42] D. Vanderbilt, *Berry Phases in Electronic Structure Theory: Electric Polarization, Orbital Magnetization and Topological Insulators* (Cambridge University Press, Cambridge, UK, 2018).

[43] A. Weiße, G. Wellein, A. Alvermann, and H. Fehske, The kernel polynomial method, Rev. Mod. Phys. **78**, 275 (2006).

[44] I. Mondragon-Shem, T. L. Hughes, J. Song, and E. Prodan, Topological criticality in the chiral-symmetric AIII class at strong disorder, Phys. Rev. Lett. **113**, 046802 (2014).

[45] J. Li, R.-L. Chu, J. K. Jain, and S.-Q. Shen, Topological Anderson insulator, Phys. Rev. Lett. **102**, 136806 (2009).

[46] C. W. Groth, M. Wimmer, A. R. Akhmerov, J. Tworzydło, and C. W. J. Beenakker, Theory of the topological Anderson insulator, Phys. Rev. Lett. **103**, 196805 (2009).

[47] M. Janssen, Multifractal analysis of broadly-distributed observables at criticality, Int. J. Mod. Phys. B **08**, 943 (1994).

[48] Z. Xiao, K. Kawabata, X. Luo, T. Ohtsuki, and R. Shindou, Anisotropic topological Anderson transitions in chiral symmetry classes, Phys. Rev. Lett. **131**, 056301 (2023).

[49] P. Zhao, Z. Xiao, Y. Zhang, and R. Shindou, Topological effect on the Anderson transition in chiral symmetry classes, Phys. Rev. Lett. **133**, 226601 (2024).